PROCEEDINGS OF SCIENCE

ICRC 2021 THE ASTROPARTICLE PHYSICS CONFERENCE Berlin | Germany 37th International Cosmic Ray Conference 12–23 July 2021

A 3D Likelihood Analysis Tool for LHAASO-KM2A data

Xiaoyuan Huang[a,*] **and Kaikai Duan**[a] **on behalf of the LHAASO Collaboration**
(a complete list of authors can be found at the end of the proceedings)

[a] *Key Laborary of Dark Matter and Space Astronomy, Purple Mountain Observatory, Yuan Hua Road, Nanjing, China*

E-mail: xyhuang@pmo.ac.cn, duankk@pmo.ac.cn

The square kilometer array (KM2A) is the main array of the Large High Altitude Air Shower Observatory (LHAASO), which is the most sensitive gamma-ray detector for energies above a few tens of TeV. We are developing a software pipeline based on the experimental data, Monte-Carlo simulations and the pointing track of the arrays. The pipeline is able to perform 3D (sky images at different energies) fits of KM2A data, similar to those used for Fermi-LAT and DAMPE gamma-ray analysis. This 3D likelihood analysis could fit source models of arbitrary morphology to the sky images, and get energy spectra information and detection significances simultaneously. The analysis with this software could give consistent results with those using traditional method.

37th International Cosmic Ray Conference (ICRC 2021)
July 12th – 23rd, 2021
Online – Berlin, Germany

*Presenter

PoS(ICRC2021)769

1. Introduction

The Large High Altitude Air Shower Observatory (LHAASO) project[1, 2] is a new generation instrument, built at 4410 meters of altitude in the Sichuan province of China, with the aim of studying the energy spectrum, the elemental composition and the anisotropy of cosmic rays in the energy range between 10^{12} and 10^{17} eV with unprecedented sensitivity, as well as to act simultaneously as a wide aperture (~2 sr), continously-operated gamma-ray telescope in the energy range between 10^{11} eV and 10^{15} eV.

As a sub-array of LHAASO, the square kilometer array (KM2A) is mainly designed to cover a large fraction of the northern sky to hunt for gamma-ray sources at energies above 10 TeV. The whole KM2A array will consist of 5195 electro-magnetic detectors (EDs, 1 m^2 each) and 1188 muon detectors (MDs, 36 m^2 each), deployed over an area of 1.3 km^2. Even though the detector construction is still underway, a half of the KM2A array has been operating stably since the end of 2019. Figure 1 shows the planed layout and the fiducial area of the current KM2A half-array used in this analysis. The atmosphere shower and detector response have been simlated for KM2A half-array, and the event reconstrucion including the core, direction and energy reconstruction and the gamma-ray/cosmic-ray discrimination have been implemented on the simulated and experimental data[3].

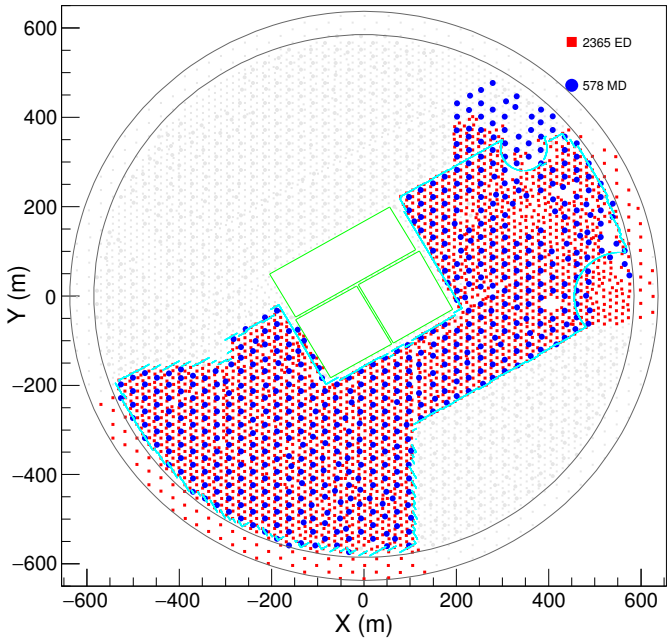

Figure 1: Planned layout of all LHAASO-KM2A detectors[3]. The red squares and blue circles indicate the EDs and MDs in operation, respectively. The area enclosed by the cyan line outlines the fiducial area of the current KM2A half-array used in this analysis.

Similar to the Fermi-LAT and DAMPE gamma-ray analysis[4], we are developing a 3D likelihood analysis software for the KM2A data. Based on the experimental data, Monte-Carlo sim-

ulations and the pointing track of the arrays, the 3D likelihood analysis counld fit source models of arbitrary morphology to the sky image, get the energy spectra information and detection significances simultaneously. The analysis with this software could give consistent results with those using traditional method[3].

2. Instrument Response Functions from Simulation Data

Instrument Response Functions (IRFs) including the effective area, point-spread function and energy dispersion represent the performance of the detections like efficiency, angular and energy resolution[5]. The effective area, $A_{\rm eff}(E, \hat{v})$, is product of the geometrical cross-section area, the efficiency of event trigger, reconstrucion and selection for gamm-ray with energy E and direction $\hat{v}$ in detector reference frame. The point spread function, $P(\hat{v}', E, \hat{v})$, and the energy dispersion, $D(E', E, \hat{v})$, are the probability distributions of the reconstructed direction $\hat{v}'$ and reconstructed energy E' for gamma-ray with energy E and direction $\hat{v}$ respectively. Given the spatial and spectral model of gamma-ray source $F(E, \hat{p})$, where $\hat{p}$ refers to the celestial direction of gamma-ray source, the expected distribution of observed gamma-ray photons is

$$r(E', \hat{p}') = \int\int\int F(E, \hat{p}) A_{\rm eff}(E, \hat{v}(t, \hat{p})) P(\hat{v}'(t, \hat{p}'), E, \hat{v}(t, \hat{p})) D(E', E, \hat{v}(t, \hat{p})) dE d\Omega dt,$$

where $\hat{p}'$ is the reconstructed celestial directions of the photons. The integrals are over the time and energy range of interest and the solid angle in the celestial reference frame.

We research the KM2A half-array IRFs for gamma-ray detection as functions of primary energy and incident angle from simulation data. The simulation gamma-ray events are sampled in the energy range from 1 TeV to 10 PeV following a powerlaw function with a spectral index of -2. The zenith angle is distributed from 0° to 70°. The sample area is a circular region with a sufficiently large radius of 1000 m. We binned the simulation data into 20 logarithm energy bins from 1 TeV to 10 PeV and 10 secant of zenith angle bins from 0° to 60°.

Effective area is the numerical function varying with energy of a gamma-ray photon and its incident direction in theinstrument reference frame. The effectivate area for the bin centering E_i and θ_j is

$$A_{\rm eff}(E_i, \theta_j) = \frac{N_{pass,i,j}}{N_{simu,i,j}} S \cos\theta_j,$$

where $N_{simu,i,j}$ and $N_{pass,i,j}$ are the number of photons generated in the simulation and passed the trigger, reconstrucion and selection. S is the sample area. Here we ignore the phi dependence of effective area. In the left panel of Figure 2 shows the effective areas in different zenith angle range.

The point spread function (PSF) is the probability distribution of the deviation between reconstructed and simlated direction $\delta v = |\hat{v}' - \hat{v}|$. We binned the deviation as the square of the angle, and get the distribution functions related with the energy and incident angle. The middle panel of Figure 2 shows some example of PSF. In the same energy, the less incident angle means the better angular resolution. In the same incident angle, the higher energy means the better angular resolution.

The energy dispersion is the distribution of reconstructed energy, it can be represented by the energy translation matrix between reconstructed and simulated energy. The right panel of

Figure 2 shows the energy translation matrix in one incident angle bin. The colorbar represents the probability density within each simualed energy bin.

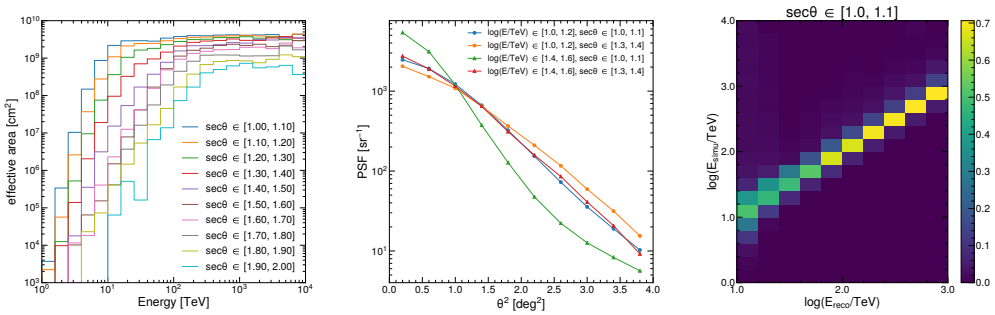

Figure 2: The IRFs obtained from the simulation gamma-ray data for KM2A half-array. The left panel is the effective area in different incident angle range, the middle panel is the PSF example in different energy and incident angle range, the right panel is the energy dispersion example in one incident angle bin.

3. Exposure and Likelihood Analysis

For a particular source in the sky, its direction in the detector reference frame varies with time. Since the IRFs vary appreciably across the KM2A's FoV, we define the exposure ϵ for any given energy E and direction in the sky $\hat{p}$ as the integral of the effective area over the time range of interest,

$$\epsilon(E, \hat{p}) = \int A_{\rm eff}(E, \hat{v}(t, \hat{p}))dt.$$

The exposure can also be expressed as an integral over the solid angle in the detector reference frame,

$$\epsilon(E, \hat{p}) = \int A_{\rm eff}(E, \hat{v}) t_{\rm obs}(\hat{v}, \hat{p}) d\Omega.$$

Here the $t_{\rm obs}$ is defined as the total time which KM2A has observed the direction $\hat{p}$ with director frame direction $\hat{v}$ during the time range of interest. Figure 3 shows the exposure map of KM2A half-array at 10 TeV in the equator coordinate with Aitoff projection.

We characterize a source by its photon flux density $F(E, \hat{p}, t; \vec{\lambda})$, here $\vec{\lambda}$ is the parameters needed to be fitted in the source model. In order to reduce the computational burden, we assume the source is stationary during the time range in each likelihood analysis. For a variable source, time dependence of the flux can be achieved by repeating the analysis in finer time bins. The model predicted photon rate in the bin ij (centered at E_i and $\hat{p}_j$) from source k is:

$$r_{ijk}(E_i', \hat{p_j'}, \vec{\lambda}_k) = \int\int F(E, \hat{p}; \vec{\lambda}_k)\epsilon(E, \hat{p})P(\hat{p_j'}, E, \hat{p})D(E_i', E, \hat{p})dE d\Omega.$$

The predicted photon distribution is compared with the observed data to determine the model parameters. We binned the data into counts cube according to the reconstructed energies and directions. For each bin, the photon number N follows a Poisson distribution with unknown mean

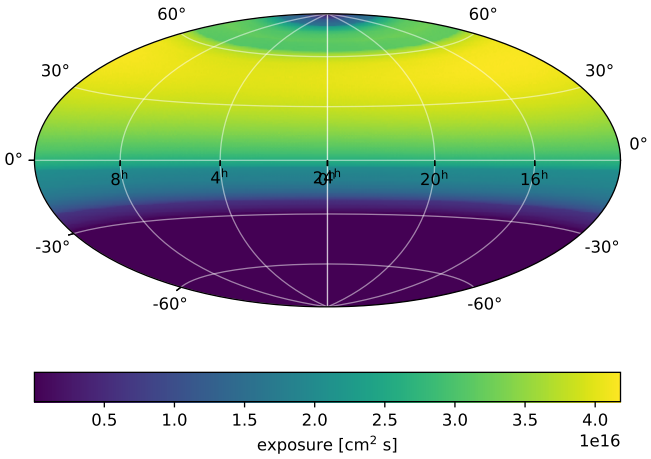

Figure 3: The exposure map of KM2A half-array at 10 TeV in the equator coordinate with Aitoff projection.

R: $p(N;R) = R^N/N!e^{-R}$. Taking into account all the bins with numbers $\{N_i\}$, the Poisson distribution becomes

$$p(\{N_i\};\{R_i\}) = \prod_{i=1}^{N_{\rm bins}} \frac{R_i^{N_i}}{N_i!} e^{-R_i}.$$

With the model predicted photon rates and the reconstructed data, and based on the Poisson statistics, we construct the binned likelihood function (in logarithm form) by summing over all $N_{\rm bins}$ bins and N_s sources

$$\log L(\vec{\lambda}) = \sum_{i,j=1}^{N_{\rm bins}} \left(-\sum_{k=1}^{N_s} R_{ijk} + N_i \log \sum_{k=1}^{N_s} R_{ijk} \right).$$

Where R_{ijk} is model expected photon numbers in bin ij from source k. By maximizing the likelihood function, we can fit the free parameters in the source model to get the best-fit values. By decreasing one from the maximal likehood value, we can get the errors of free parameters. The confidence level of source k is described by the test statistics

$$TS_k = -2(\log L(\vec{\lambda}_{0,k}) - \log L(\vec{\lambda}_0)),$$

where the $\vec{\lambda}_0$ is the best-fit value of model parameters and $\vec{\lambda}_{0,k}$ is the best-fit parameters without the source k includes in the model. The TS_k follows a χ^2 distribution with $h-m$ degrees of freedom[6], where h and m are the number of free parameters in the model with/out source k.

4. Implementation and examples

The code is written with python, based on the NumPy[7], SciPy[8], AstroPy[9], and Minuit[10] package. For expandability, the software are structured with modules. The input modules include `SkyMap`, `IRFs`, `SpatialModel`, `Spectrum`, `Model` and `fitRegion`. The process modules include `Exposure`, `Source`, `LikelihoodBase` and `BinnedLikelihood`. `LikelihoodAnalysis`

is the ouput module. We also provide some scripts for users including `plotCountsMap.py`, `plotfitRegion.py`, `plotSpatailModel.py`, `plotSpectrum.py` and `BinnedAnalysis.py`. The fitRegion and model file are described with YAML format.

As examples, Figure 4 shows the counts map around the Crab Nebula binned with 0.1*0.1 degree^2 with CAR projection and fit region around Cygnus Cocoon which is in a 6° radius circle region around (RA=307.17°, DEC=41.17°) and removed a 1.5° radius circle region around (RA=304.85°, DEC=36.80°) plotted with `plotCountsMap.py` and `plotfitRegion.py` scripts.

Figure 5 shows the spataial map which is a extended source centered at (RA=307.65°, DEC=40.93°) with a Gaussian width of 2.13° and power-law spectrum $dN/dE = N_0(E/E_0)^{\Gamma}$ with $N_0 = 9.3\times10^{-13}$ cm^{-2}s^{-1}TeV^{-1}, $\Gamma = -2.64$, $E_0 = 4.2$ TeV of Cygnus Cocoon[11] plotted with `plotSpatialModel.py` and `plotSpectrum.py` scripts.

Figure 6 shows the spectral energy distribution (SED) and test statistics (TS) map of the Crab Nebula fitted with `BinnedAnalysis.py`. Compared with the results in [3], the analysis with this software could give consistent results with those using traditional method.

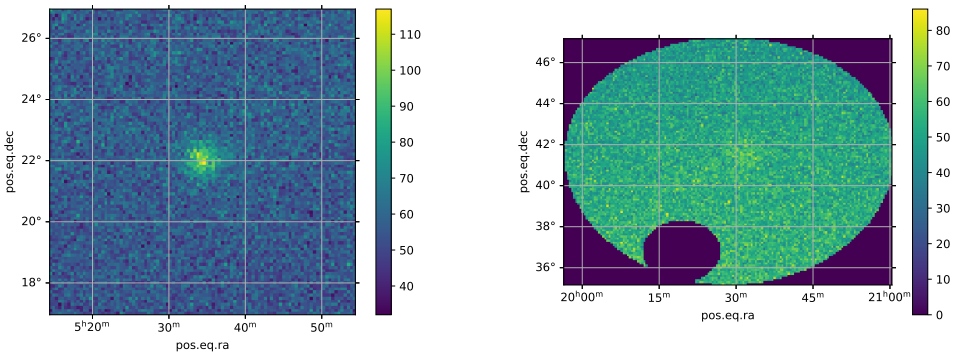

Figure 4: Left panel shows the counts map around the Crab Nebula binned with 0.1*0.1 degree^2 with CAR projection, right panel shows the fit region around Cygnus Cocoon which is in a 6° radius circle region around (RA= 307.17°, DEC=41.17°) and removed a 1.5° radius circle region around (RA=304.85°, DEC=36.80°).

5. Summary

The very-high-energy gamma-ray sky is an important observation target for KM2A, the sub-array of LHAASO. To facilitate analyzing the KM2A gamma-ray data, we have developed a dedicated software, which implements maximum likelihood analysis to extract the parameters of sources that contribute to the observed gamma-rays. The KM2A IRFs that are essential to the gamma-ray data analysis, including the effective area, PSF and energy dispersion, are also derived based on statistics from simulation data. Applying the KM2A IRFs and the software that are detailed in this paper, scientific analyses of the gamma-ray data could be carried out to obtain the best-fit spectral parameters, fluxes and corresponding statistical uncertainties, and further the spectral energy distribution, promoting our understanding of the nature of very-high-energy gamma-ray phenomena.

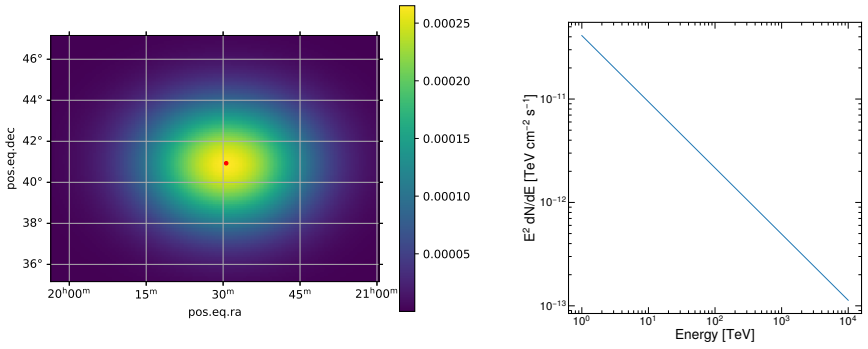

Figure 5: Cygnus Cocoon spatial map which is a extended source centered at (RA=307.65°, DEC=40.93°) with a Gaussian width of 2.13° and power-law spectrum $dN/dE = N_0(E/E_0)^{\Gamma}$ with $N_0 = 9.3 \times 10^{-13}$ cm^{-2}s^{-1}TeV^{-1}, $\Gamma = -2.64$, $E_0 = 4.2$ TeV of Cygnus Cocoon[11].

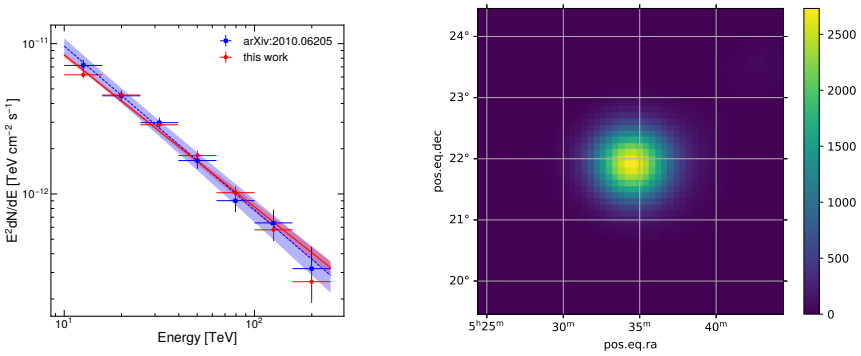

Figure 6: The spectral energy distribution (SED) and test statistics (TS) map of the Crab Nebula.

References

[1] Cao Z., *A future project at tibet: the large high altitude air shower observatory (LHAASO)*, *Chinese Phys. C*, 34, 249 (2010).

[2] Bai X., Bi B. Y., Bi X. J. et al., *The Large High Altitude Air Shower Observatory (LHAASO) Science White Paper*, *arXiv:1905.02773*.

[3] Aharonian F., An Q., Axikegu, et al., *The observation of the Crab Nebula with LHAASO-KM2A for the performance study*, *Chin. Phys. C*, 45, 025002 (2021).

[4] Duan K. K., Jiang W., Liang Y. F., et al., *DmpIRFs and DmpST: DAMPE instrument response functions andsciencetools for gamma-ray data analysis*, *Research in Astronomy and Astrophysics*, 19, 132 (2019).

[5] Ackermann, M., Ajello, M., Albert, A., et al., *The Fermi Large Area Telescope on orbit: event classification, instrument response functions, and calibration.*, *Astrophys. Jour. Supp.*, 203, 4 (2012).

[6] Wilks, S. S., *The Large-Sample Distribution of the Likelihood Ratio for Testing Composite Hypotheses.*, *Ann. Math. Statist.*, 9, 60 (1938).

[7] Harris, Charles R., Millman K. Jarrod, et al., *Array programming with NumPy*, *Nat.*, 585, 357 (2020).

[8] Virtanen P., Gommers R., et al., *SciPy 1.0: Fundamental Algorithms for Scientific Computing in Python*, *Nat. Methods*, 17, 261 (2020).

[9] Robitaille, T. P., Tollerud, E. J., Greenfield, P., et al., *Astropy: A community Python package for astronomy*, *Astronomy and Astrophysics*, 558, 33 (2013).

[10] James, F. and Roos, M. *Minuit – A System for Function Minimization and Analysis of the Parameter Errors and Correlations*, *Comp. Phy. Comm.*, 10, 343 (1975).

[11] Abeysekara A.U., Albert A., Alfaro R. et al., *HAWC observations of the acceleration of very-high-energy cosmic rays in the Cygnus Cocoon*, *Nat. Astron.*, 5, 465 (2021).

Full Authors List: LHAASO Collaboration

Zhen Cao[1,2,3], F. Aharonian[4,5], Q. An[6,7], Axikegu[8], L.X. Bai[9], Y.X. Bai[1,3], Y.W. Bao[10], D. Bastieri[11], X.J. Bi[1,2,3], Y.J. Bi[1,3], H. Cai[12], J.T. Cai[11], Zhe Cao[6,7], J. Chang[13], J.F. Chang[1,3,6], B.M. Chen[14], E.S. Chen[1,2,3], J. Chen[9], Liang Chen[15], Long Chen[8], M.J. Chen[1,3], M.L. Chen[1,3,6], Q.H. Chen[8], S.H. Chen[1,2,3], S.Z. Chen[1,3], T.L. Chen[16], X.L. Chen[1,2,3], Y. Chen[10], N. Cheng[1,3], Y.D. Cheng[1,3], S.W. Cui[14], X.H. Cui[17], Y.D. Cui[18], B. D'Ettorre Piazzoli[19], B.Z. Dai[20], H.L. Dai[1,3,6], Z.G. Dai[7], Danzengluobu[16], D. della Volpe[21], X.J. Dong[1,3], K.K. Duan[13], J.H. Fan[11], Y.Z. Fan[13], Z.X. Fan[1,3], J. Fang[20], K. Fang[1,3], C.F. Feng[22], L. Feng[13], S.H. Feng[1,3], Y.L. Feng[13], B. Gao[1,3], C.D. Gao[22], L.Q. Gao[1,2,3], Q. Gao[16], W. Gao[22], M.M. Ge[20], L.S. Geng[1,3], G.H. Gong[23], Q.B. Gou[1,3], M.H. Gu[1,3,6], F.L. Guo[15], J.G. Guo[1,2,3], X.L. Guo[8], Y.Q. Guo[1,3], Y.Y. Guo[1,2,3,13], Y.A. Han[24], H.H. He[1,2,3], H.N. He[13], J.C. He[1,2,3], S.L. He[11], X.B. He[18], Y. He[8], M. Heller[21], Y.K. Hor[18], C. Hou[1,3], X. Hou[25], H.B. Hu[1,2,3], S. Hu[9], S.C. Hu[1,2,3], X.J. Hu[23], D.H. Huang[8], Q.L. Huang[1,3], W.H. Huang[22], X.T. Huang[22], X.Y. Huang[13], Z.C. Huang[8], F. Ji[1,3], X.L. Ji[1,3,6], H.Y. Jia[8], K. Jiang[6,7], Z.J. Jiang[20], C. Jin[1,2,3], T. Ke[1,3], D. Kuleshov[26], K. Levochkin[26], B.B. Li[14], Cheng Li[6,7], Cong Li[1,3], F. Li[1,3,6], H.B. Li[1,3], H.C. Li[1,3], H.Y. Li[7,13], Jian Li[7], Jie Li[1,3,6], K. Li[1,3], W.L. Li[22], X.R. Li[1,3], Xin Li[8], Y. Li[9], Y.Z. Li[1,2,3], Zhe Li[1,3], Zhuo Li[27], E.W. Liang[28], Y.F. Liang[28], S.J. Lin[18], B. Liu[7], C. Liu[1,3], D. Liu[22], H. Liu[8], H.D. Liu[24], J. Liu[1,3], J.L. Liu[29], J.S. Liu[18], J.Y. Liu[1,3], M.Y. Liu[16], R.Y. Liu[10], S.M. Liu[8], W. Liu[1,3], Y. Liu[11], Y.N. Liu[23], Z.X. Liu[9], W.J. Long[8], R. Lu[20], H.K. Lv[1,3], B.Q. Ma[27], L.L. Ma[1,3], X.H. Ma[1,3], J.R. Mao[25], A. Masood[8], Z. Min[1,3], W. Mitthumsiri[30], T. Montaruli[21], Y.C. Nan[22], B.Y. Pang[8], P. Pattarakijwanich[30], Z.Y. Pei[11], M.Y. Qi[1,3], Y.Q. Qi[14], B.Q. Qiao[1,3], J.J. Qin[7], D. Ruffolo[30], V. Rulev[26], A. Sáiz[30], L. Shao[14], O. Shchegolev[26,31], X.D. Sheng[1,3], J.R. Shi[1,3], H.C. Song[27], Yu.V. Stenkin[26,31], V. Stepanov[26], Y. Su[13], Q.N. Sun[8], X.N. Sun[28], Z.B. Sun[32], P.H.T. Tam[18], Z.B. Tang[6,7], W.W. Tian[2,17], B.D. Wang[1,3], C. Wang[32], H. Wang[8], H.G. Wang[11], J.C. Wang[25], J.S. Wang[29], L.P. Wang[22], L.Y. Wang[1,3], R.N. Wang[8], W. Wang[12], X.G. Wang[28], X.J. Wang[1,3], X.Y. Wang[10], Y. Wang[8], Y.D. Wang[1,3], Y.J. Wang[1,3], Y.P. Wang[1,2,3], Z.H. Wang[9], Z.X. Wang[20], Zhen Wang[29], Zheng Wang[1,3,6], D.M. Wei[13], J.J. Wei[13], Y.J. Wei[1,2,3], T. Wen[20], C.Y. Wu[1,3], H.R. Wu[1,3], S. Wu[1,3], W.X. Wu[8], X.F. Wu[13], S.Q. Xi[1,3], J. Xia[7,13], J.J. Xia[8], G.M. Xiang[2,15], D.X. Xiao[16], G. Xiao[1,3], H.B. Xiao[11], G.G. Xin[12], Y.L. Xin[8], Y. Xing[15], D.L. Xu[29], R.X. Xu[27], L. Xue[22], D.H. Yan[25], J.Z. Yan[13], C.W. Yang[9], F.F. Yang[1,3,6], J.Y. Yang[18], L.L. Yang[18], M.J. Yang[1,3], R.Z. Yang[7], S.B. Yang[20], Y.H. Yao[9], Z.G. Yao[1,3], Y.M. Ye[23], L.Q. Yin[1,3], N. Yin[22], X.H. You[1,3], Z.Y. You[1,2,3], Y.H. Yu[22], Q. Yuan[13], H.D. Zeng[13], T.X. Zeng[1,3,6], W. Zeng[20], Z.K. Zeng[1,2,3], M. Zha[1,3], X.X. Zhai[1,3], B.B. Zhang[10], H.M. Zhang[10], H.Y. Zhang[22], J.L. Zhang[17], J.W. Zhang[9], L.X. Zhang[11], Li Zhang[20], Lu Zhang[14], P.F. Zhang[20], P.P. Zhang[14], R. Zhang[7,13], S.R. Zhang[14], S.S. Zhang[1,3], X. Zhang[10], X.P. Zhang[1,3], Y.F. Zhang[8], Y.L. Zhang[1,3], Yi Zhang[1,13], Yong Zhang[1,3], B. Zhao[8], J. Zhao[1,3], L. Zhao[6,7], L.Z. Zhao[14], S.P. Zhao[13,22], F. Zheng[32], Y. Zheng[8], B. Zhou[1,3], H. Zhou[29], J.N. Zhou[15], P. Zhou[10], R. Zhou[9], X.X. Zhou[8], C.G. Zhu[22], F.R. Zhu[8], H. Zhu[17], K.J. Zhu[1,2,3,6], X. Zuo[1,3]

[1]Key Laboratory of Particle Astrophyics & Experimental Physics Division & Computing Center, Institute of High Energy Physics, Chinese Academy of Sciences, 100049 Beijing, China.
[2]University of Chinese Academy of Sciences, 100049 Beijing, China.
[3]TIANFU Cosmic Ray Research Center, Chengdu, Sichuan, China.
[4]Dublin Institute for Advanced Studies, 31 Fitzwilliam Place, 2 Dublin, Ireland .
[5]Max-Planck-Institut for Nuclear Physics, P.O. Box 103980, 69029 Heidelberg, Germany.
[6]State Key Laboratory of Particle Detection and Electronics, China.
[7]University of Science and Technology of China, 230026 Hefei, Anhui, China.
[8]School of Physical Science and Technology & School of Information Science and Technology, Southwest Jiaotong University, 610031 Chengdu, Sichuan, China.
[9]College of Physics, Sichuan University, 610065 Chengdu, Sichuan, China.
[10]School of Astronomy and Space Science, Nanjing University, 210023 Nanjing, Jiangsu, China.
[11]Center for Astrophysics, Guangzhou University, 510006 Guangzhou, Guangdong, China.
[12]School of Physics and Technology, Wuhan University, 430072 Wuhan, Hubei, China.
[13]Key Laboratory of Dark Matter and Space Astronomy, Purple Mountain Observatory, Chinese Academy of Sciences, 210023 Nanjing, Jiangsu, China.
[14]Hebei Normal University, 050024 Shijiazhuang, Hebei, China.
[15]Key Laboratory for Research in Galaxies and Cosmology, Shanghai Astronomical Observatory, Chinese Academy of Sciences, 200030 Shanghai, China.
[16]Key Laboratory of Cosmic Rays (Tibet University), Ministry of Education, 850000 Lhasa, Tibet, China.
[17]National Astronomical Observatories, Chinese Academy of Sciences, 100101 Beijing, China.
[18]School of Physics and Astronomy & School of Physics (Guangzhou), Sun Yat-sen University, 519000 Zhuhai, Guangdong, China.
[19]Dipartimento di Fisica dell'Università di Napoli 'Federico II", Complesso Universitario di Monte Sant'Angelo, via Cinthia, 80126 Napoli, Italy. .
[20]School of Physics and Astronomy, Yunnan University, 650091 Kunming, Yunnan, China.
[21]D'epartement de Physique Nucl'eaire et Corpusculaire, Facult'e de Sciences, Universit'e de Genève, 24 Quai Ernest Ansermet, 1211 Geneva, Switzerland.
[22]Institute of Frontier and Interdisciplinary Science, Shandong University, 266237 Qingdao, Shandong, China.
[23]Department of Engineering Physics, Tsinghua University, 100084 Beijing, China.
[24]School of Physics and Microelectronics, Zhengzhou University, 450001 Zhengzhou, Henan, China.
[25]Yunnan Observatories, Chinese Academy of Sciences, 650216 Kunming, Yunnan, China.
[26]Institute for Nuclear Research of Russian Academy of Sciences, 117312 Moscow, Russia.

PoS(ICRC2021)769

[27]School of Physics, Peking University, 100871 Beijing, China.
[28]School of Physical Science and Technology, Guangxi University, 530004 Nanning, Guangxi, China.
[29]Tsung-Dao Lee Institute & School of Physics and Astronomy, Shanghai Jiao Tong University, 200240 Shanghai, China.
[30]Department of Physics, Faculty of Science, Mahidol University, 10400 Bangkok, Thailand.
[31]Moscow Institute of Physics and Technology, 141700 Moscow, Russia.
[32]National Space Science Center, Chinese Academy of Sciences, 100190 Beijing, China.